JOURNAL OF APPLIED POLYMER SCIENCE VOL. 19, PP. 1755–1766 (1975)

Polypropylene Fibers Melt-Spun in the Presence of Torsional Shear

P. G. ANDERSEN, S. TEST, S. R. DEO, and S. H. CARR,
Department of Materials Science, Northwestern University, Evanston, Illinois 60201

Synopsis

Melt-spun fibers of isotactic polypropylene have been formed using specific combinations of shearing and elongational flow. Such rheological conditions were achieved with a take-up device capable of subjecting molten polymer filaments continuously to various combinations of torsional and elongational strains. Relationships were determined between mechanical properties of the resulting fibers and their molecular organizations. The results obtained indicated that these flow fields would produce fibers whose mean-preferred-chain-orientation directions ranged between being tilted radially from a direction parallel with the fiber axis (no torsional shear strain imposed) and having some additional tilt that is tangential with respect to the fiber circumference (some torsional shear strain imposed). It is not possible to resolve the observed helical chain tilts into contributions from crystalline and amorphous regions, respectively.

INTRODUCTION

Information regarding what happens to molten polymer as it moves down a fiber-spinning thread line can be obtained from recent research focusing on such areas as changes in fiber diameter, development of optical retardation, variation of surface temperature,[1] rheological phenomena,[2–4] and heat-transfer effects.[5,6] Work seeking to relate resulting microstructures with conditions that exist during the fiber-spinning process has shown[7,8] that elongational flow is the predominant mode by which molten filaments deform as they become supercooled and undergo solidification. If the deformation rate achieved is small, the character of preferred orientation is weak,[9–10] but as this rate is increased, the magnitude of preferred orientation is observed to strengthen. In addition, because the viscous compliance of material is lowest in the cooler, exterior parts of a molten filament, there is a tendency for some amount of shearing flow to occur by relative motion between concentric cylindrical elements.[11,12] Microstructures in the resulting fibers have been shown[8,12] to consist of parallel lamellae that are all essentially perpendicular to the fiber axis, although the polymer chains are known to have some systematic, radially inward tilt to their orientation.

Such a microstructure is typical of those produced whenever polymers are solidified in the presence of flow. Earlier studies on crystallization from flowing melts and solutions[13–21] demonstrated that if chains became sufficiently oriented,

then crystallization would occur at lower amounts of undercooling and would produce solids whose microstructures had corresponding preferred orientations. More recently, it was recognized[22] that crystallization would occur first in certain localities of flow fields where some elongational character exists, and as a result, the notion emerges that elongational flow is more effective than shearing flow in causing flow-induced crystallization. Yet, in most technical polymer-processing operations, the kinds of flow fields employed are of mixed elongational and shearing character, so the results reported here were obtained from work designed to examine solids formed in the presence of flows produced by combining uniaxial elongations with torsional shears on unconstrained molten polymer filaments.

EXPERIMENTAL

Hexane-extracted Profax 6523F (Hercules, Inc., Wilmington, Del.) isotactic polypropylene was used in the preparation of all fiber samples. Simple melt-spun fibers (i.e., no torsional shear applied) were produced as described previously by Fung et al.[11] This involved extruding the polymer melted at 205°C from an Instron Capillary Rheometer at continuous rates and allowing molten filaments, which were cooled by convective heat transfer to ambient air, to crystallize as they underwent extensions ranging from 17 to 200×. Fibers spun in the presence of torsional shear experienced the same processing except a steady

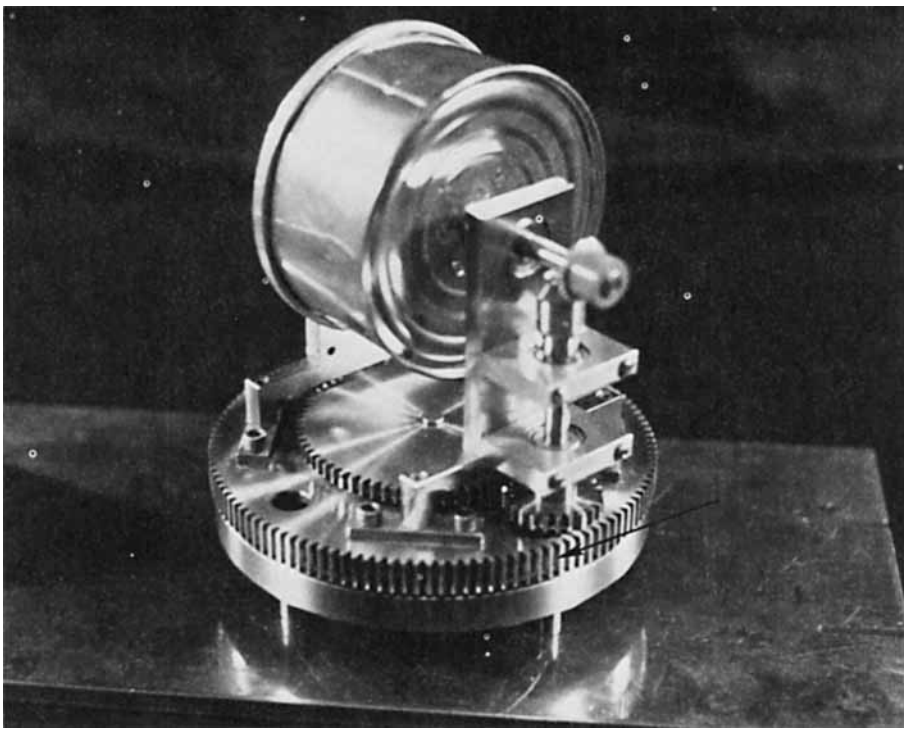

Fig. 1. The take-up device that melt-spins fibers using a combination of elongational and shearing flows. A 4-in. diameter drum, which rotates about its own cylindrical axis, creates the desired amounts of filament elongation (draw-down), and the torsional shear is achieved by driving the large gear (arrow) that, in turn, rotates the platform on which the take-up drum is mounted.

twisting strain, $\dot{\gamma}$, was superimposed onto the extensional rate. This torsional shear strain could be applied at rates between 0 and 250 rpm. The apparatus used to produce the torsional shear and extension rates is shown in Figure 1. It is a 4-in. diameter take-up drum that can be driven at variable speeds to rotate about its own cylindrical axis and thereby generate purely uniaxial extensional flow in the molten polymer filament. Torsional shear is achieved by rotating the large gear (arrow), which, in turn, causes the take-up drum to spin about its vertical axis. Varying the speeds of these two rotations independently allows different combinations of torsional shear and extension rates to be produced.

Birefringence measurements were made for various fiber preparations on 10-μ-thick cross sections obtained by standard microtomy of fibers imbedded in Spur resin. Profiles of birefringence parallel to the original fiber axis were obtained along an arbitrary diameter using a polarizing optical microscope fitted with a Berek compensator. Specimens were then tilted 10° from the horizontal using the arbitrary diameter along which the initial profiles were measured as the tilt axis. Subsequently, a new profile across that diameter displaying maximum enhancement of these birefringence values was recorded.

Measurements of the complex elastic modulus, E, its real and imaginary components, E' and E'', and the loss tangent, tan δ, of fibers prepared by these techniques were made, as previously described,[23] on a Rheovibron Model DDV-II dynamic-mechanical tester (Toyo Measuring Instrument Co. Ltd., Tokyo, Japan).

Wide-angle x-ray diffraction photographs were taken of all the samples before and after testing on the Rheovibron. These photographs were taken in a cylindrical camera using nickel-filtered CuK_α radiation at 40 kV from a Phillips x-ray unit.

RESULTS AND DISCUSSION

Examination of polypropylene fibers that had been melt spun under various combinations of torsional shear and elongational strain revealed evidence regarding the actual character of flow responsible for their crystallization. Because the viscous compliance of material along the threadline varies from essentially zero in solidified polymer to some readily measured value for melt as it emerges from the spinneret, one must presume that permanent deformation imposed by the take-up device occurs almost entirely within unfrozen material. This resulting flow has a character that must lie somewhere between the two cases shown in Figures 2a and 2b. Each illustration depicts a portion of the molten filament in the region where flow is experienced; evidence for each limiting situation has been observed. In support of the one case, fiber cross sections have revealed a series of concentric rings centered about the fiber axis (just like growth rings in a tree), possibly indicating flow of the kind illustrated in Figure 2a. This torsional shearing flow has velocity that is a function of r and not of z (as in a couette viscometer). On the other hand, careful examination of some fibers reveals the existence of helical bumps running along their surfaces. This may be interpreted as evidence for the other kind of flow, where circumferential velocity is a function of z and not r (as in the parallel plate viscometer). Finally, it is important to note that in either case the superposition of shear flow does

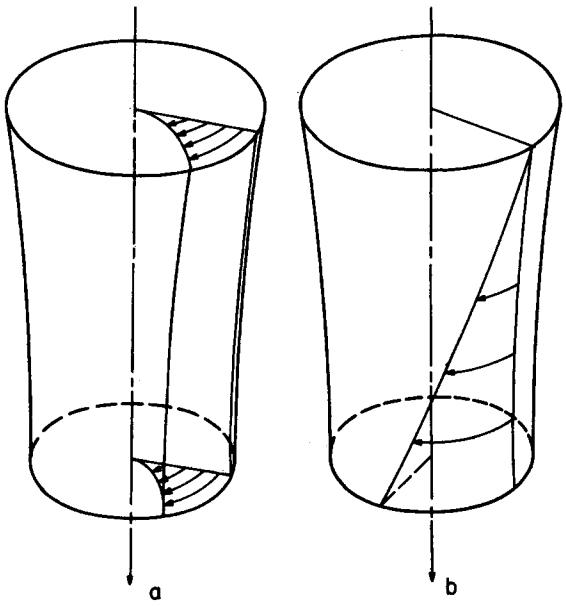

Fig. 2. Schematic representation of a portion of molten filament showing two possible modes of shearing flow: (a) torsion creates a velocity gradient that varies with radius but not axial position and (b) torsion creates a velocity gradient that varies with axial position but is independent of radial location. In either case, the filament undergoes a fixed amount of elongation (vertical direction).

not affect the draw-down ratio of the fiber; this has been verified experimentally by measurements of fiber diameters.

Varying the magnitude of torsional shearing flow superimposed onto a given level of elongational strain ratio is illustrated by the four x-ray diffraction patterns shown in Figures 3a–3d. Where no torsional shear has been applied (Fig. 3a), it is seen that the 110 reflections indicate only a modest orientation. Applying a 50-rpm twist to the fiber (Fig. 3b) produces a definite maximum on the innermost equatorial reflection, indicating increased orientation of the microstructure. Increasing the superposed twist further (Figs. 3c and 3d) enhances the orientation, as shown by the development of two distinct 110 meridional reflections from a continuous, nearly uniform intensity diffraction arc. Additional evidence of increased orientation resulting from superposed torsional shear is presented in Figure 4. It shows dynamic–mechanical tensile loss moduli plotted as functions of temperature for the same samples as those used for Figure 3. These data indicate that increasing torsional shear from 0 to 200 rpm causes the tensile modulus and loss tangent to increase by approximately 30%. This is consistent with recent work of Andersen and Carr,[23] who showed that increased microstructural orientation due to applied elongational strain is accompanied by an increase in both mechanical properties.

Although x-ray diffraction patterns show that orientation of primary population crystallites, as well as second population crystallites,[23] increased with torsional shear rate, birefringence values produced from 10-μ-thick fiber cross sections reveal additional information regarding these microstructures. Figure 5 shows a comparison of birefringence values for two such samples which were

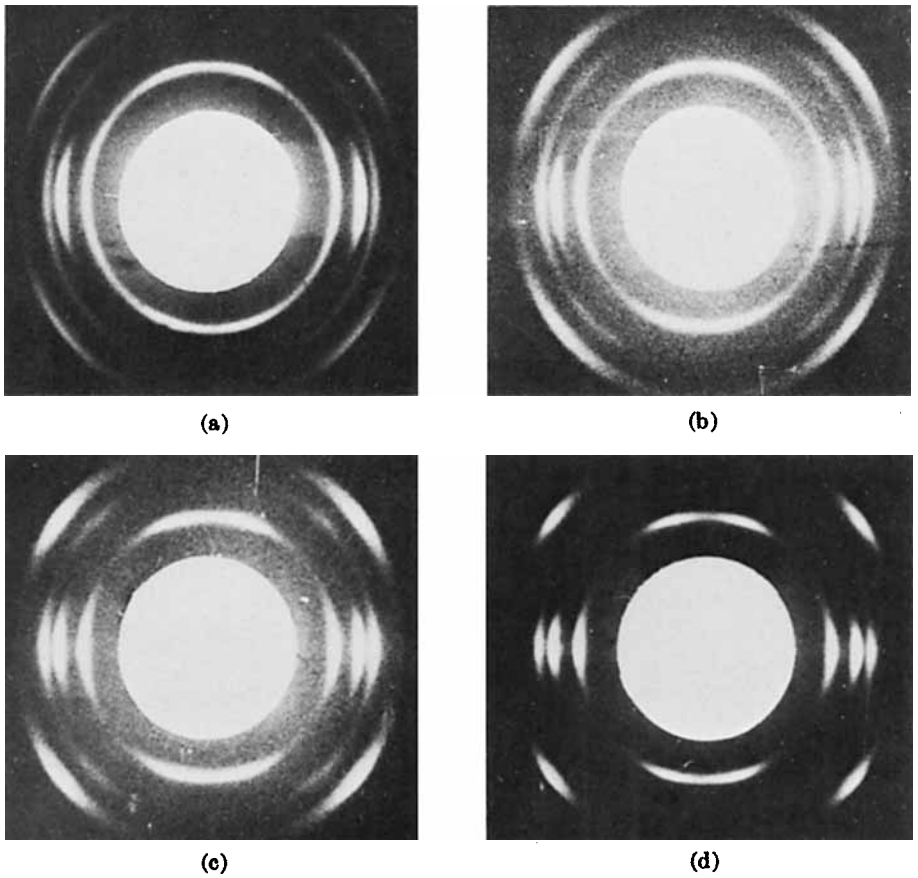

Fig. 3. Four x-ray diffraction photographs from fibers spun with a single draw-down ratio, E, of 43, and different levels of torsional shear rates. Judging from the nonuniformity of the 110 reflections, which make the innermost ring, it is seen that there is a progressive increase in preferred orientation as torsion is increased: (*a*) $\dot{\gamma} = 0$; (*b*) $\dot{\gamma} = 50$ rpm; (*c*) $\dot{\gamma} = 150$ rpm; and (*d*) $\dot{\gamma} = 200$ rpm. Fiber axis is vertical.

subjected to equal strain but different torsional shear rates. The solid line shows a radial distribution of birefringence values taken along an arbitrary sample diameter and measured parallel to the fiber axis. These resulting values must be due to molecular chains being tilted somewhat with respect to the optic axis, since viewing them parallel to their axis would yield nearly zero birefringence. It was found that fibers for which no torsion was applied contained chains tilted slightly inward in a radial manner. Birefringence measurements also revealed that fibers formed at low draw-down ratios had an inner core of spherulitic material surrounded by an outer core of flow-crystallized microstructure, as revealed by x-ray analysis. Because the material on the fiber exterior experiences the most rapid cooling, it is expected that the flow-crystallized surface layers solidified first. This would produce a local shear at the melt/solid interface and would produce a radially inward chain tilt in part, or all, of the microstructure.

However, in cases where torsional shear was present, it is suspected that this chain tilt may have some helical character to it, as well. To determine whether

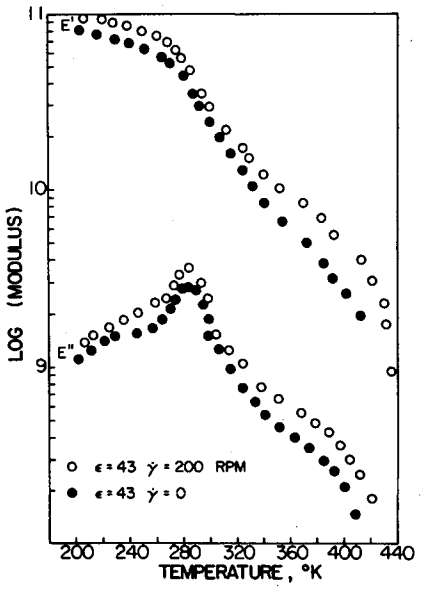

Fig. 4. The temperature dependence of real, E', and imaginary, E'', components of the complex tensile modulus for two specimens represented in Figure 3. It can be seen that increasing torsional shear rate, while holding elongation rate constant, causes an increase in both kinds of moduli.

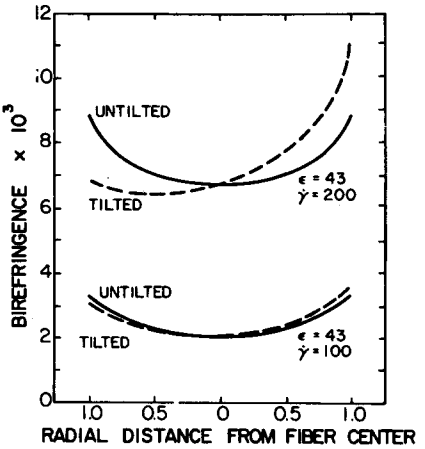

Fig. 5. Birefringence measured parallel to the fiber axis for two samples from the set represented in Figure 3. Radial position is expressed as a fractional parameter. Tilting the entire microtomed section on the optical microscope stage causes birefringence to increase in one quadrant of the specimen and to decrease in the opposite quadrant: (——) birefringence profile for an untilted specimen, (– – –) that birefringence profile which, after the tilting process exhibits the largest difference in birefringence when going from one side to the other.

this hypothesis is correct for a given fiber, its entire microtomed section was tilted. If the chain tilt were only radial, one would expect that extinction and enhancement of birefringence values would be seen in quadrants opposite to each other across the specimen tilt axis, as illustrated schematically in Figure 6. If, on the other hand, chain tilt were only helical, extinction and enhancement

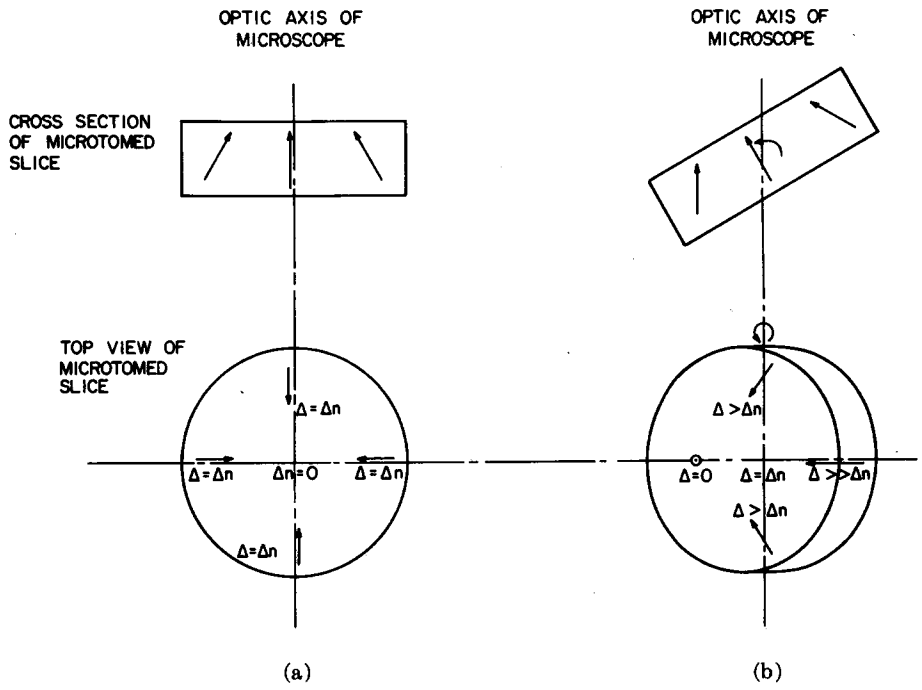

Fig. 6. Schematic representations of a microtomed section from a fiber in which average chain orientation has a radially inward inclination. The birefringence, Δ, would be the same value, Δn, for any given radial position, as shown in (a), but if the specimen were tilted as in (b), the birefringence along a line perpendicular to the specimen tilt axis would increase strongly on one side and possibly go to zero on the opposite. Arrows represent projections of local chain orientation directions onto the views shown.

would be found only along the speciman tilt axis, as shown in Figure 7. What was actually observed was that for samples subjected to only an extensional strain, extinction and enhancement did occur along a line perpendicular to the tilt axis. However, for twist-spun fibers with a mixed flow field, the quadrants which become extinct or enhanced were located between the two extremes. As an example, these quadrants are found along a line that is 30° from the specimen tilt axis for the fiber represented in Figure 4, and the magnitudes of birefringence as functions of radial position along this particular diameter are shown in Figure 5.

Further experimentation to determine the tilt angle at which maximum enhancement and extinction occur would allow quantitative identification of chain tangential and radial tilt components. By imagining an exaggerated top view along the fiber axis, as shown in Figure 8, it can be seen that at two points the actual chain tilt will lie in a plane parallel to that made by the x-direction and the fiber axis. By slight rotation of the microtomed section about its y-axis, birefringence at one point is enhanced, while at the opposite point extinction occurs. The maximum extinction and enhancement occur at these points because the chains are perpendicular to the tilt axis. This line is situated at some angle, φ, from the x-axis. There also exists a specimen tilt angle, ψ, at which the difference between extinction and enhancement of birefringence is strongest. This angle is equal to the average chain direction shown in Figure 9.

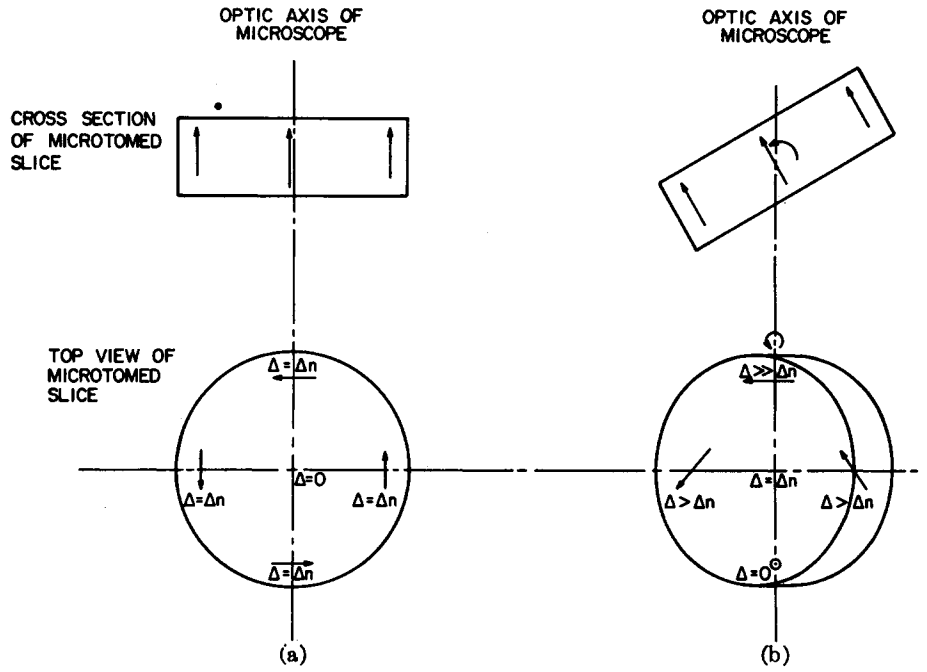

Fig. 7. Schematic representations of a microtomed section from a fiber in which average chain orientation has a tangential inclination. The birefringence, Δ, would be the same value, Δn, for any given radial position, as shown in (a), but if the specimen were tilted as in (b), the birefringence along a line parallel to the specimen tilt axis would increase strongly on one side and possibly go to zero on the opposite. Arrows represent projections of local chain orientation directions onto the views shown.

Once ψ and φ are known, simple geometry enables the following relationship to be developed for the radial component of chain tilt:

$$\cot r = \cot \psi / \cos \varphi$$

Similarly, the tangential chain tilt component, t, is,

$$\cot t = \cot \psi / \sin \varphi$$

X-Ray diffraction analysis and dynamic-mechanical testing revealed that results for the two fiber samples shown in Figures 10 and 11 were very interesting. One specimen was formed using purely elongational strain, while the other underwent half as much strain but was subjected to a 150-rpm torsional shear component. Figure 10 shows that the resulting crystal textures in these two samples have qualitatively identical preferred orientations. However, Figure 11 reveals that, although real parts of their tensile moduli are almost the same, there is a difference between imaginary parts of their moduli in the temperature range where loss processes are predominantly due to chains in amorphous regions. If one envisions the average orientation distribution function for chain segments in amorphous regions to be represented by an ellipsoidal figure, then the magnitude of preferred orientation would be proportional to its ratio of major to minor axes, and the characteristic direction of this orientation would be the angle, χ, between its major axis and the specimen fiber axis. It is expected that χ is larger for fibers spun in the presence of torsion, in which case both

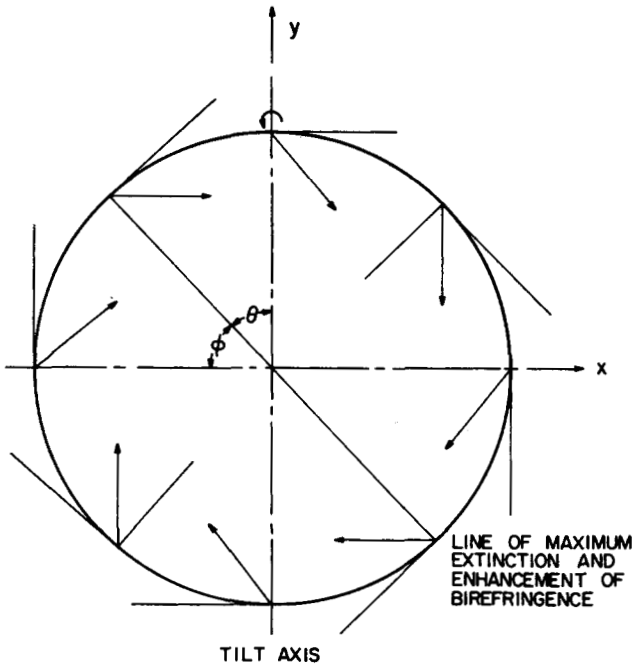

Fig. 8. Schematic representation of the top of a microtomed section from a fiber in which average chain orientation has an inclination that is a combination of tangential and radial components. When such a specimen is tilted on the optical microscope stage, the maximum extinction and enhancement of birefringence will occur along some diagonal line, as is indicated in this figure. Arrows around the circumference represent projections of local chain orientation directions onto this top view.

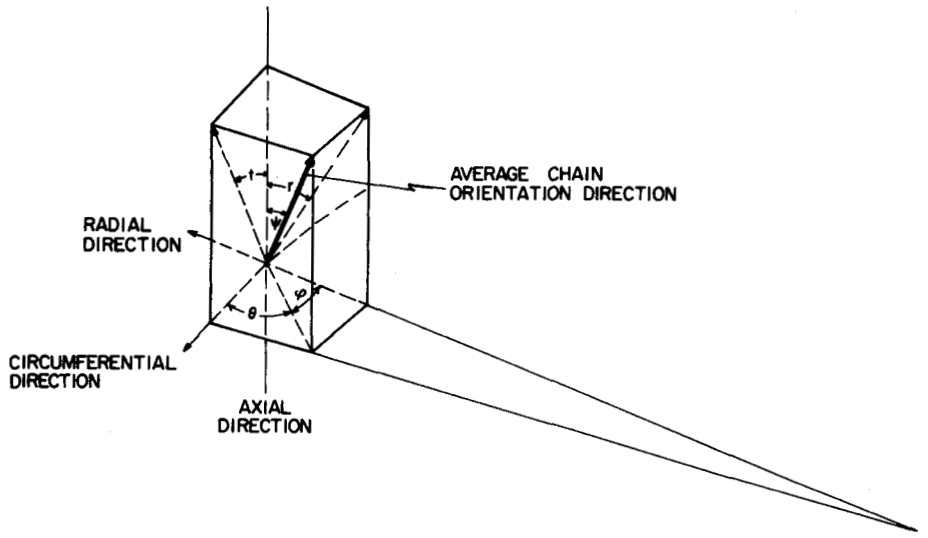

Fig. 9. Angular relationships between local chain orientation direction (heavy arrow) and coordinate axes of a fiber. The average chain orientation is inclined from the fiber axis by an angle, ψ, which can be resolved into a tangential component, t, and a radial component, r. The projection of the chain orientation direction seen in a top view is φ from the radial direction or θ from the circumferential direction.

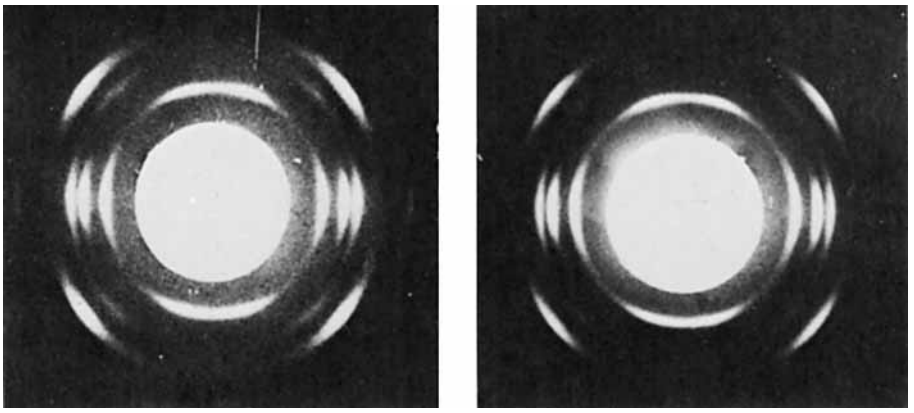

(a) (b)

Fig. 10. X-Ray diffraction photographs for two fibers having essentially equivalent crystal textures. The one for a was spun using a draw-down ratio of 43 and a torsional shear rate, $\dot{\gamma}$, of 150 rpm, while the one for b, which was spun without torsional shear, required twice the elongation in order to achieve the same preferred orientation.

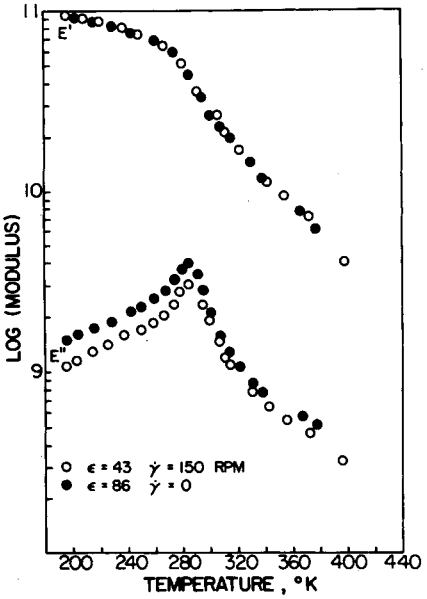

Fig. 11. Dynamic mechanical data for the same fibers used in the previous figure, where both were shown to have essentially the same crystal textures. It is seen here, likewise, that both have the same values of E' over the temperature range studied. However, the peak in E'' located around 280°K, which is due to motions in noncrystalline regions, is slightly larger for fibers spun with torsion, when compared to their background, than this peak is for those fibers spun without torsion.

angles t and r would contribute to χ, than for fibers spun in the absence of torsion, in which case the angle t would be zero. As a result, stresses involved in dynamic–mechanical tests are applied at oblique angles to amorphous chain segments in fibers spun with some shear present; but in fibers spun without torsional shear, these stresses are applied more nearly parallel to amorphous chain segments

(χ is smaller). In previous studies on highly drawn polypropylene solids, Owen and Ward[24] measured the effects on loss modulus of stressing such amorphous chains in a parallel or perpendicular manner. In this work they showed that loss modulus in this temperature range would be greatest if stresses were applied parallel to the orientation direction. Consequently, the observation in work reported here that the loss modulus at 23°C is lower for fibers made with rather than without torsion may be regarded as evidence for there being more strongly tilted amorphous chains in fibers of the former rather than the latter kind. However, the extent to which similar orientation effects for chains in crystals may account for part of the chain tilt (radial plus tangential) birefringence cannot be established on the basis of available data, but it is expected that there must be some finite contribution from this source as well.

CONCLUSIONS

Draw-down of molten polypropylene filaments in the presence of torsional shearing deformation superimposed onto a main elongational deformation creates a combined shearing and elongational flow field along the spin line. This resulting complex flow field greatly enhances the ensuing preferred orientation of lamellar crystallites compared to orientation produced by equivalent amounts of purely extensional flow. It has also been shown that there is a helicoidal nature to the preferred orientations of both crystallites and amorphous chains. Thus, as a result of the increased preferred orientation there exists a corresponding increase in the tensile modulus of material subjected to torsional shear. The consequence of this fact is that fibers of larger cross-sectional area and higher modulus can be produced from the same fiber-spinning process simply by adding a torsional shear component to the flow field.

The authors wish to express their appreciation for financial support of this work from the National Science Foundation through the Northwestern Materials Research Center.

References

1. A. B. Thompson, in *Fiber Structure*, J. W. S. Hearle and R. H. Peters, Eds., Butterworth, London, 1963, Chapt. 14.
2. A. Ziabicki, *Kolloid-Z. Z. Polym.*, **14**, 175 (1961).
3. S. Kose and T. Matsuo, *J. Polym. Sci. A*, **3**, 2541 (1965).
4. T. Ishibashi, K. Aoki, and T. Ishii, *J. Appl. Polym. Sci.*, **14**, 1597 (1970).
5. E. H. Andrews, *Brit. J. Appl. Phys.*, **10**, 39 (1959).
6. D. Acierno, J. N. Dalton, J. M. Rodriguez, and J. L. White, *J. Appl. Polym. Sci.*, **15**, 2395 (1971).
7. T. Manabe, *J. Appl. Polym. Sci.*, **8**, 1097 (1964).
8. K. Katayama, T. Amano, and K. Nakamura, *Kolloid-Z. Z. Polym.*, **226**, 125 (1968).
9. R. J. Samuels, *Structured Polymer Properties*, Wiley, New York, 1974, pp. 140–158.
10. T. Kitao, S. Ohya, J. Furukawa, and S. Yamashita, *J. Polym. Sci. A-2*, **11**, 1091 (1973).
11. P. Y.-F. Fung, E. Orlando, and S. H. Carr, *Polym. Eng. Sci.*, **13**, 295 (1973).
12. P. Y.-F. Fung and S. H. Carr, *J. Macromol. Sci., Phys.*, **B6**, 621 (1972).
13. A. Keller and M. J. Machin, *J. Macromol. Sci., Phys.*, **B1**, 41 (1967).
14. M. J. Hill and A. Keller, *J. Macromol. Sci., Phys.*, **B3**, 153 (1969).
15. A. J. Pennings, J. M. A. A. van der Mark, and A. M. Kiel, *Kolloid-Z. Z. Polym.*, **237**, 336 (1970).
16. R. B. Williamson and W. F. Busse, *J. Appl. Phys.*, **38**, 4187 (1967).
17. T. Kawai, T. Matsumoto, M. Koto, and H. Maeda, *Kolloid-Z. Z. Polym.*, **222**, 1 (1968).
18. K. Kobayaski and T. Nagosawa, *J. Macromol. Sci., Phys.*, **B4**, 331 (1970).

19. T. W. Haas and B. Maxwell, *Polym. Eng. Sci.*, **9**, 225 (1969).
20. T. Kawai, M. Iguchi, H. Tonami, *Kolloid-Z. Z. Polym.*, **221**, 28 (1967).
21. R. J. Samuels, *J. Polym. Sci. C*, **20**, 253 (1967).
22. S. Matsuzawa, K. Yamaura, and H. Yanagisawa, *Kolloid-Z. Z. Polym.*, **250**, 20 (1972).
23. P. G. Andersen and S. H. Carr, *J. Materials Sci.*, in press.
24. A. J. Owen and I. M. Ward, *J. Macromol. Sci., Phys.*, **B7**, 417 (1973).

Received October 3, 1974